Sensing-Aided Uplink Channel Estimation for Joint Communication and Sensing

Xu Chen, *Member, IEEE*, Zhiyong Feng, *Senior Member, IEEE*, J. Andrew Zhang, *Senior Member, IEEE*, Zhiqing Wei, *Member, IEEE*, Xin Yuan, *Member, IEEE*, and Ping Zhang, *Fellow, IEEE*

***Abstract*—The joint communication and sensing (JCAS) technique has drawn great attention due to its high spectrum efficiency by using the same transmit signal for both communication and sensing. Exploiting the correlation between the uplink (UL) channel and the sensing results, we propose a sensing-aided Kalman filter (SAKF)-based channel state information (CSI) estimation method for UL JCAS, which exploits the angle-of-arrival (AoA) estimation to improve the CSI estimation accuracy. A Kalman filter (KF)-based CSI enhancement method is proposed to refine the least-square CSI estimation by exploiting the estimated AoA as the prior information. Simulation results show that the bit error rates (BER) of UL communication using the proposed SAKF-based CSI estimation method approach those using the minimum mean square error (MMSE) method, while at significantly reduced complexity.**

***Index Terms*—Sensing-aided communication, 6G, joint communication and sensing, Kalman Filter.**

I. Introduction

JOINT communication and sensing (JCAS) is regarded as one of the most promising techniques for dealing with the spectrum congestion problem in the future 6G networks, achieving wireless communication and sensing using the same transmit signals [1], [2], [3]. The uplink (UL) JCAS estimates sensing parameters from the UL channel state information (CSI) [4]. Therefore, the CSI is highly related to the environment sensing information such as the angle-of-arrival (AoA), delay (or range), and Doppler frequency for the signals between the base station (BS) and the user. Moreover, the CSI estimation is critical for realizing reliable communications.

Manuscript received 20 November 2022; accepted 11 December 2022. Date of publication 16 December 2022; date of current version 9 March 2023. This work was supported in part by the National Key Research and Development Program of China under Grant 2020YFA0711300, Grant 2020YFA0711302, and Grant 2020YFA0711303; in part by the National Natural Science Foundation of China under Grant 61941102 and Grant 61790553; and in part by the BUPT Excellent Ph.D. Students Foundation under Grant CX2021110. The associate editor coordinating the review of this article and approving it for publication was I. Al-Nahhal. *(Corresponding author: Zhiyong Feng.)*

Xu Chen, Zhiyong Feng, and Zhiqing Wei are with the Key Laboratory of Universal Wireless Communications, Ministry of Education, Beijing University of Posts and Telecommunications, Beijing 100876, China (e-mail: chenxu96330@bupt.edu.cn; fengzy@bupt.edu.cn; weizhiqing@bupt.edu.cn).

J. Andrew Zhang is with the Global Big Data Technologies Centre, University of Technology Sydney, Sydney, NSW 2007, Australia (e-mail: Andrew.Zhang@uts.edu.au).

Xin Yuan is with the Data61, Commonwealth Scientific and Industrial Research Organization, Sydney, NSW 2121, Australia (e-mail: Xin.Yuan@data61.csiro.au).

Ping Zhang is with the State Key Laboratory of Networking and Switching Technology, Beijing University of Posts and Telecommunications, Beijing 100876, China (e-mail: pzhang@bupt.edu.cn).

Digital Object Identifier 10.1109/LWC.2022.3229660

The least-square (LS) method has been widely utilized for channel estimation due to its low complexity [5]. Nevertheless, its low CSI estimation accuracy may result in a large signal-to-noise ratio (SNR) loss for communications. To deal with this problem, the minimum mean square error (MMSE) method was proposed to improve the CSI estimation accuracy. However, the high complexity makes it challenging to be utilized in real applications [6].

Moreover, using the communication signals to estimate the sensing parameters, such as Doppler frequency, delay, AoA, and angle-of-departure (AoD), has attracted great attention. In [7], the authors proposed a joint AoA and Doppler frequency estimation method and used the AoA and Doppler estimation to conduct channel tracking and compensate for the Doppler shift. In [8], the authors jointly estimated the partial angular-domain channel and Doppler frequency offset (DFO), and a DFO compensation method was proposed based on the estimates. In [9], the authors proposed to use a tensor decomposition-based method to estimate the Doppler frequency, delay, AoA, and AoD. Moreover, the authors proposed a joint AoD and Doppler shift estimation method that iteratively refines the AoD and Doppler estimation. However, this method has a high complexity.

The CSIs can be treated as sequences containing amplitude fading and phase shifts, which are related to angular, time, and frequency domain indices. Kalman filter (KF) can suppress the varying noise terms in a sequence defined as state transfer [10]. In this letter, we propose a sensing-aided Kalman filter (SAKF)-based CSI estimation method for UL JCAS. Exploiting the estimated AoAs as the prior information to construct the CSI state transfer, we use a KF to iteratively suppress the noise terms in the initial CSI estimation. The improved CSI estimate leads to the smaller bit error rate (BER). Note that UL JCAS can estimate sensing parameters including AoA, Doppler frequency, delay, etc., nevertheless, we only choose the AoA estimate as the prior information. This is because it is hard to obtain accurate Doppler and delay estimates in the presence of the carrier frequency offset (CFO) and timing offset (TO) [4]. Comparatively, AoA changes slowly and its estimation is not impacted by CFO and TO. Simulation results show that the proposed SAKF-based CSI estimation method can achieve BER performance approaching that of the MMSE method.

Notations: Bold uppercase letters denote matrices (e.g., $\mathbf{M}$); bold lowercase letters denote column vectors (e.g., $\mathbf{v}$); scalars are denoted by normal font (e.g., γ); the entries of vectors or matrices are referred to with square brackets; $(\cdot)^*$ and $(\cdot)^T$ denote Hermitian transpose, complex conjugate and transpose, respectively; $\mathbf{M}_1 \in \mathbb{C}^{M\times N}$ and $\mathbf{M}_2 \in \mathbb{R}^{M\times N}$ are $M \times N$ complex-value and real-value matrices, respectively; for two

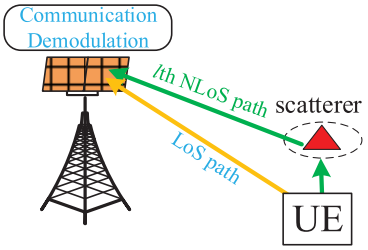

Fig. 1. The UL JCAS scenario.

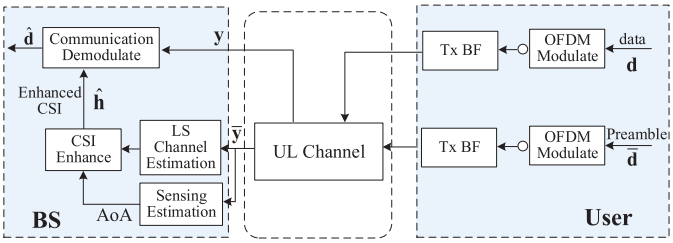

Fig. 2. The UL JCAS scheme with the SAKF-based CSI estimation.

given matrices $\mathbf{S}1$ and $\mathbf{S}2$, $[v_{p,q}]|_{(p,q)\in\mathbf{S}1\times\mathbf{S}2}$ denotes the vector stacked by values $v_{p,q}$ satisfying $p \in \mathbf{S}1$ and $q \in \mathbf{S}2$; and $v \sim \mathcal{CN}(m, \sigma^2)$ means v follows a complex Gaussian distribution with mean m and variance σ^2.

II. System Model

This section presents the UL JCAS system setup, and received signal model to provide fundamentals for demonstrating the SAKF-based CSI estimation method.

A. UL JCAS System Setup

We consider a UL JCAS system, where the BS and the user equipment (UE) are equipped with uniform plane arrays (UPAs), as shown in Fig. 1. UE moves at a low-to-medium speed.[1] In the UL preamble (ULP) period, UE transmits the UL preamble signals, and BS uses the received training sequences in the preamble for CSI estimation, and the estimated CSI is further used to estimate sensing parameters. In the UL data (ULD) period, the BS demodulates the UL data signals of UE using the estimated CSI. For simplicity of presentation, we assume that there is one ULP in each packet for CSI estimation, and the ULPs are transmitted at an equal interval, denoted by T_s^p.

Orthogonal frequency division multiplexing (OFDM) signal is adopted as the transmit signal. The key parameters for the OFDM signal are denoted as follows. P_t^U is the transmit power, N_c is the number of subcarriers occupied by UE; M_s is the number of OFDM packets used for each sensing parameter estimation; $d_{n,m}$ is the transmit OFDM baseband symbol of the mth OFDM symbol at the nth subcarrier, f_c is the carrier frequency, Δf is the subcarrier interval, T_s is the time duration of each OFDM symbol, $T_s^p = P_s T_s$, and P_s is the number of OFDM symbols in each packet. The sensing parameter estimates are updated every M_s packets.

B. UPA Model

This subsection presents the UPA model. The uniform interval between neighboring antenna elements is denoted by d_a. The size of UPA is $P \times Q$. The AoA for receiving or the angle-of-departure (AoD) for transmitting the kth far-field signal is $\mathbf{p}_k = (\varphi_k, \theta_k)^T$, where φ_k and θ_k are the azimuth and elevation angles, respectively. The phase difference between the (p, q)th antenna element and the reference antenna element is

$$a_{p,q}(\mathbf{p}_k) = \exp\left[-j\frac{2\pi}{\lambda} d_a(p\cos\varphi_k \sin\theta_k + q\sin\varphi_k \sin\theta_k)\right], \quad (1)$$

[1]The velocity of UE is no larger than 120 km/h.

where $\lambda = c/f_c$ is the wavelength of the carrier, and c is the speed of light. The steering vector for the array is given by

$$\mathbf{a}(\mathbf{p}_k) = [a_{p,q}(\mathbf{p}_k)]\big|_{p=0,1,\ldots,P-1;q=0,1,\ldots,Q-1}, \quad (2)$$

where $\mathbf{a}(\mathbf{p}_k) \in \mathbb{C}^{PQ\times 1}$. The sizes of the antenna arrays of the BS and the user are $P_t \times Q_t$ and $P_r \times Q_r$, respectively.

C. Received Signal Model

The frequency-domain received communication signal at the nth subcarrier of the mth OFDM symbol is expressed as [4]

$$\mathbf{y}_{C,n,m} = \sqrt{P_t^U} d_{n,m} \sum_{l=0}^{L-1} \begin{bmatrix} e^{j2\pi m T_s^p [f_{c,d,l}+\delta_f(m)]} \\ e^{-j2\pi n \Delta f [\tau_{c,l}+\delta_\tau(m)]} \\ \times b_{C,l}\chi_{TX,l}\mathbf{a}(\mathbf{p}_{RX,l}^U) \end{bmatrix} + \mathbf{n}_{n,m}, \quad (3)$$

where $l = 0$ is for the channel response of the LoS path, and $l \in \{1, \ldots, L-1\}$ is for the lth non-LoS (NLoS) path; $\chi_{TX,l} = \mathbf{a}^T(\mathbf{p}_{TX,l}^U)\mathbf{w}_{TX}$ is the transmit BF gain, $\mathbf{w}_{TX} \in \mathbb{C}^{P_r Q_r \times 1}$ is the transmit beamforming (BF) vector, and $\mathbf{a}(\mathbf{p}_{TX,l}^U) \in \mathbb{C}^{P_r Q_r} \times 1$ and $\mathbf{a}(\mathbf{p}_{RX,l}^U) \in \mathbb{C}^{P_t Q_t} \times 1$ are the steering vectors for UL transmission and receiving, respectively; $f_{c,d,l}$ and $\tau_{c,l}$ are the Doppler and delay of the lth path, respectively; $\delta_f(m)$ and $\delta_\tau(m)$ are the carrier frequency offset (CFO) and timing offset (TO), respectively; $\delta_f(m)$ and $\delta_\tau(m)$ are random time-varying parameters, and are assumed to follow $\mathcal{CN}(0, \sigma_f^2)$ and $\mathcal{CN}(0, \sigma_\tau^2)$, respectively; $b_{C,l}$ is the reflection factor for the lth path with $b_{C,0} = 1$ being the LoS path's reflection factor and $b_{C,l}$ $(l > 0)$ being a random variable following $\mathcal{CN}(0, \sigma_{\beta_l}^2)$; $\mathbf{n}_{n,m}$ is the combined noise including Gaussian noise and possible reflected interferences, and each element of $\mathbf{n}_{n,m}$ follows $\mathcal{CN}(0, \sigma_N^2)$; and $\mathbf{y}_{C,n,m}, \mathbf{n}_{n,m} \in \mathbb{C}^{P_t Q_t \times 1}$.

III. SAKF-Based CSI Estimation Method

In this section, we present the SAKF-based CSI estimation method. The UL JCAS scheme is shown in Fig. 2. In the ULP period, the UL CSI estimation at the nth subcarrier of the mth OFDM symbol is obtained via the LS method [5] as

$$\hat{\mathbf{h}}_{C,n,m} = \frac{\mathbf{y}_{C,n,m}}{d_{n,m}} = \mathbf{h}_{C,n,m} + \bar{\mathbf{n}}_{n,m} \in {}^{P_t Q_t \times 1}$$
$$= \sum_{l=0}^{L-1} \begin{bmatrix} e^{j2\pi m T_s^p [f_{c,d,l}+\delta_f(m)]} \\ e^{-j2\pi n \Delta f [\tau_{c,l}+\delta_\tau(m)]} \\ \sqrt{P_t^U} b_{C,l}\chi_{TX,l}\mathbf{a}(\mathbf{p}_{RX,l}^U) \end{bmatrix} + \bar{\mathbf{n}}_{n,m}. \quad (4)$$

where $\mathbf{y}_{C,n,m}$ is given in (3), $\mathbf{h}_{C,n,m}$ is the actual equivalent CSI, and $d_{n,m}$ is the preamble symbol with unit constant modulus.

A. AoA Estimation

We utilize the multiple signal classification (MUSIC) method to estimate AoAs. We stack all $M_s \times N_c$ CSI estimates (from N_c subcarriers and M_s packets) to obtain the matrix $\hat{\mathbf{H}}_C \in \mathbb{C}^{P_t Q_t \times N_c M_s}$, where the $[(m-1)N_c+n]$th column of $\hat{\mathbf{H}}_C$ is $\hat{\mathbf{h}}_{C,n,m}$. Construct the correlation matrix of $\hat{\mathbf{H}}_C$ as

$$\begin{aligned}\mathbf{R_x} &= [\hat{\mathbf{H}}_C(\hat{\mathbf{H}}_C)^H]/(M_s N_c)\\ &= \sum_{m,n} \hat{\mathbf{h}}_{C,n,m}(\hat{\mathbf{h}}_{C,n,m})^H/(M_s N_c),\end{aligned} \tag{5}$$

According to the definition of $\hat{\mathbf{h}}_{C,n,m}$, we can see that $\mathbf{R_x}$ does not contain $e^{j2\pi m T_s^p \delta_f(m)} e^{-j2\pi n \Delta f \delta_\tau(m)}$. Specifically, $e^{j2\pi m T_s^p \delta_f(m)} e^{-j2\pi n \Delta f \delta_\tau(m)}$ is compensated in $E\{\mathbf{h}_{C,n,m}(\mathbf{h}_{C,n,m})^H\}$ given m; for $E\{\mathbf{h}_{C,n,m}\bar{\mathbf{n}}_{n,m}\}$, the expectations of the multiplication of noise and $e^{j2\pi m T_s^p \delta_f(m)} e^{-j2\pi n \Delta f \delta_\tau(m)}$ are 0. Therefore, the AoA estimation is not prominently affected by the CFO and TO, while it is a challenging issue for estimating the range and Doppler [4]. Thus, AoA is the most suitable sensing parameter to refine the communication CSI.

Referenced to [11], applying eigenvalue decomposition to $\mathbf{R_x}$, we can obtain the eigen matrix as $\mathbf{U}_x$, and the noise subspace of $\mathbf{R_x}$ is $\mathbf{U}_N = [\mathbf{U}_x]_{:,L+1:P_t Q_t}$, where $\mathbf{U}_s = [\mathbf{U}]_{:,N_1:N_2}$ indicates the matrices sliced from the N_1th to the N_2th columns of $\mathbf{U}$, and L is the number of identified incident signals that can be determined by the minimum description length (MDL) method [12]. Then, the angle spectrum function can be obtained as [11]

$$f_a(\mathbf{p}) = \mathbf{a}^H(\mathbf{p})\mathbf{U}_N(\mathbf{U}_N)^H\mathbf{a}(\mathbf{p}). \tag{6}$$

Finally, the minimum points of $f_a(\mathbf{p})$ are found as the AoA estimates. Let $\hat{\mathbf{p}}_{RX,l}^U = (\hat{\varphi}_l, \hat{\theta}_l), l \in \{0,\ldots,L-1\}$ denote the lth AoA estimate.

B. KF-Based CSI Enhancement Method

Reshape $\hat{\mathbf{h}}_{C,n,m} \in \mathbb{C}^{P_t Q_t \times 1}$ into $\hat{\mathbf{H}}_{C,n,m} \in \mathbb{C}^{P_t \times Q_t}$, and $\mathbf{h}_{C,n,m} \in \mathbb{C}^{P_t Q_t \times 1}$ into $\mathbf{H}_{C,n,m} \in \mathbb{C}^{P_t \times Q_t}$. According to (3), if we treat the incident signal in the lth AoA as the observing signal, then $[\hat{\mathbf{H}}_{C,n,m}]_{p,q}$ can be rewritten as

$$\begin{aligned}[\hat{\mathbf{H}}_{C,n,m}]_{p,q} &= [\mathbf{H}^l_{C,n,m}]_{p,q} + [\mathbf{I}^l_{n,m}]_{p,q} + n^{p,q}_{n,m}\\ &= \sqrt{P_t^U}\alpha_{n,m,l} e^{-j\frac{2\pi}{\lambda}d_a(p\cos\varphi_l \sin\theta_l + q\sin\varphi_l\sin\theta_l)}\\ &\quad + [\mathbf{I}^l_{n,m}]_{p,q} + n^{p,q}_{n,m},\end{aligned} \tag{7}$$

where $\alpha_{n,m,l} = b_{C,l} e^{j2\pi m T_s \tilde{f}_{d,l,m}} e^{-j2\pi n \Delta f \tilde{\tau}_{l,m}} \chi_{TX,l}$, $\tilde{f}_{d,l,m} = f_{c,d,l} + \delta_f(m)$, $\tilde{\tau}_{l,m} = \tau_{c,l} + \delta_\tau(m)$, and $n^{p,q}_{n,m} = [\bar{\mathbf{n}}_{n,m}]_{pQ_t+q}$. Moreover, $[\mathbf{I}^l_{n,m}]_{p,q}$ is the interference signals from other paths, as given by

$$[\mathbf{I}^l_{n,m}]_{p,q} = \sqrt{P_t^U}\sum_{i=0,i\neq l}^{L-1} \alpha_{n,m,i} e^{-j\frac{2\pi d_a}{\lambda}(p\cos\varphi_i\sin\theta_i + q\sin\varphi_i\sin\theta_i)}. \tag{8}$$

According to (7), we can treat $[\hat{\mathbf{H}}_{C,n,m}]_{p,q}$ as the noisy observation of $[\mathbf{H}^l_{C,n,m}]_{p,q}$. Let $\hat{A}_{P,l} = e^{-j\frac{2\pi}{\lambda}d_a\cos\hat{\varphi}_l\sin\hat{\theta}_l}$ and $\hat{A}_{Q,l} = e^{-j\frac{2\pi}{\lambda}d_a\sin\hat{\varphi}_l\sin\hat{\theta}_l}$ denote the state transfer factors. Then, according to (7), the state transfer of $\mathbf{H}^l_{C,n,m}$ in the p-axis and q-axis are expressed, respectively, as

$$[\hat{\mathbf{H}}_{C,n,m}]_{p+1,q} = [\hat{\mathbf{H}}_{C,n,m}]_{p,q}\hat{A}_{P,l} + \Delta_{P,l}, \tag{9}$$

$$[\hat{\mathbf{H}}_{C,n,m}]_{p,q+1} = [\hat{\mathbf{H}}_{C,n,m}]_{p,q}\hat{A}_{Q,l} + \Delta_{Q,l}, \tag{10}$$

where $\Delta_{P,l} \approx ([\mathbf{I}^l_{n,m}]_{p,q} + n^{p,q}_{n,m})\hat{A}_{P,l}$ and $\Delta_{Q,l} \approx ([\mathbf{I}^l_{n,m}]_{p,q} + n^{p,q}_{n,m})\hat{A}_{Q,l}$ are the noise terms varying with the antenna-domain indices p and q. Therefore, each row and column of $\hat{\mathbf{H}}_{C,n,m}$ can be filtered by a KF to suppress the noise in (7). Let $\hat{\mathbf{h}}_C$ and $\bar{\mathbf{h}}_C$ denote a row or a column of $\hat{\mathbf{H}}_{C,n,m}$ and its filtered vector, respectively. The prior estimation of $[\hat{\mathbf{h}}_C]_p$ can be expressed as

$$[\hat{\mathbf{h}}_C]_p^- = [\hat{\mathbf{h}}_C]_{p-1}A, for\ p \in \{1,\ldots,P-1\}, \tag{11}$$

where $A = \hat{A}_{P,l}$ or $\hat{A}_{Q,l}$ when $[\hat{\mathbf{h}}_C]_p$ is a column or a row vector, respectively. Then, $[\bar{\mathbf{h}}_C]_p$ can be further updated as [10]

$$[\bar{\mathbf{h}}_C]_p = [\hat{\mathbf{h}}_C]_p^- + K_p([\hat{\mathbf{h}}_C]_p - [\hat{\mathbf{h}}_C]_p^-), \tag{12}$$

where K_p is the data fusion factor. Moreover, K_p is expressed as [10]

$$\begin{aligned}K_p &= (p_{w,p}^-)^*(p_{w,p}^- + \sigma_N^2)^{-1},\\ p_{w,p}^- &= A p_{w,p-1} A^*,\\ p_{w,p} &= (1-K_p)p_{w,p}^-,\end{aligned} \tag{13}$$

where σ_N^2 is the power of the interference-plus-noise, its estimation is $\hat{\sigma}_N^2$,[2] and $p_{w,0}$ is the variance of initial observation. Based on (9) and (10), we can estimate $p_{w,0}$ as

$$p_{w,0} \approx \frac{1}{P}\sum_{p=0}^{P-1} |[\hat{\mathbf{h}}_C]_p(A)^{-p} - [\hat{\mathbf{h}}_C]_0|_2^2. \tag{14}$$

Based on (11)-(14), we propose the KF-based CSI enhancement method as shown in **Algorithm 1**. Note that we further add an inverse version of KF in **Step** 5, where the transfer factor is updated as A^{-1}. **Step** 5 is necessary because it takes several iterations for KF in **Step** 4 to suppress the noise terms steadily. Therefore, the initially processed terms in **Step** 4 may still contain large noise. The reverse iterations of KF in **Step** 5 can update these non-ideal terms. By exploiting the estimated AoAs of JCAS as the prior information, **Algorithm 1** can suppress the noise terms in (7).

By using **Algorithm 1** to filter Q_t columns of $\hat{\mathbf{H}}_{C,n,m}$ in parallel with $\hat{A}_{P,l}$, we can obtain $\hat{\mathbf{H}}^{l,(1)}_{C,n,m}$. Further, we can also use **Algorithm 1** to filter the pth row of $\hat{\mathbf{H}}^{l,(1)}_{C,n,m}$ by replacing the input with $A = \hat{A}_{Q,l}$ and $\hat{\mathbf{h}}_C = [\hat{\mathbf{H}}^{l,(1)}_{C,n,m}]_{p,:}$. After filtering all P_t rows of $\hat{\mathbf{H}}^{l,(1)}_{C,n,m}$, we obtain $\hat{\mathbf{H}}^{l,(2)}_{C,n,m}$.

After obtaining all the $\hat{\mathbf{H}}^{l,(2)}_{C,n,m}$ for $l = 0,\ldots,L-1$, the aggregation of all L channel components is given by

$$\hat{\mathbf{H}}^{(2)}_{C,n,m} = \sum_{l=0}^{L-1}\hat{\mathbf{H}}^{l,(2)}_{C,n,m}. \tag{15}$$

[2]it can be estimated as the mean value of the last $P_t Q_t - L$ eigenvalues of $\mathbf{R_x}$ [11].

Algorithm 1: KF-Based CSI Enhancement Method

Input: The observation variance $\sigma_N^2 = \hat{\sigma}_N^2$; The transfer factor $A = \hat{A}_p$; The observation sequence $\hat{\mathbf{h}}_C = [\hat{\mathbf{H}}^l_{C,n,m}]_{:,q}$.
Output: Filtered sequence $\bar{\mathbf{h}}_C$.
Step 1: The dimension of $\hat{\mathbf{h}}_C$ is obtained as P;
Step 2: $[\bar{\mathbf{h}}_C]_0 = [\hat{\mathbf{h}}_C]_0$;
Step 3: $p_{w,0} = \frac{1}{P}\sum_{p=0}^{P-1} |[\hat{\mathbf{h}}_C]_p (A)^{-p} - [\hat{\mathbf{h}}_C]_0|_2^2$;
Step 4:
for $p = 1$ *to* $P-1$ **do**
  $[\hat{\mathbf{h}}_C]_p^- = A[\bar{\mathbf{h}}_C]_{p-1}$;
  $p_{w,p}^- = A p_{w,p-1} A^*$;
  $K_p = \left(p_{w,p}^-\right)^* (p_{w,p}^- + \sigma_N^2)^{-1}$;
  $[\bar{\mathbf{h}}_C]_p = [\hat{\mathbf{h}}_C]_p^- + K_p([\hat{\mathbf{h}}_C]_p - [\hat{\mathbf{h}}_C]_p^-)$;
  $p_{w,p} = (1 - K_p) p_{w,p}^-$;
end
Step 5: **for** $p = P-1$ *to* 1 **do**
  $[\hat{\mathbf{h}}_C]_{p-1}^- = A^{-1}[\bar{\mathbf{h}}_C]_p$;
  $p_{w,p-1}^- = A^{-1} p_{w,p} (A^{-1})^*$;
  $K_p = (p_{w,p-1}^-)^* (p_{w,p-1}^- + \sigma_N^2)^{-1}$;
  $[\bar{\mathbf{h}}_C]_{p-1} = [\hat{\mathbf{h}}_C]_{p-1}^- + K_p([\hat{\mathbf{h}}_C]_{p-1} - [\hat{\mathbf{h}}_C]_{p-1}^-)$;
  $p_{w,p-1} = (1 - K_p) p_{w,p-1}^-$;
end
return $\bar{\mathbf{h}}_C$.

After being filtered by **Algorithm 1**, the noise term in the CSI estimation will be suppressed. Vectorize $\hat{\mathbf{H}}^{(2)}_{C,n,m}$ as $\hat{\mathbf{h}}^{(2)}_{C,n,m} = vec(\hat{\mathbf{H}}^{(2)}_{C,n,m}) \in \mathbb{C}^{P_t Q_t \times 1}$. Then, we can use $\hat{\mathbf{h}}^{(2)}_{C,n,m}$ to demodulate UL data signals with zero-forcing (ZF) receive BF [5].

The reasons that we choose AoA as the prior information rather than Doppler or delay estimates are as follows. The CSIs containing CFO and TO phase shifts are required for communication demodulation. It is complicated to accurately estimate the Doppler-plus-CFO and Delay-plus-TO at each packet. Even if we acquire the accurate Doppler and delay estimates at each packet, the CFO and TO can introduce unexpected errors into CSI enhancement procedures in **Algorithm 1**. Therefore, we choose AoA estimation as the prior information for KF to enhance the CSI estimation.

C. Complexity Analysis

In this subsection, we analyze the complexity of the above SAKF-based CSI estimation. The CSI estimation of the MMSE method can be expressed as [5]

$$\hat{\mathbf{h}}_{MMSE} = \mathbf{R_{hh}}\left[\mathbf{R_{hh}} + \hat{\sigma}_N^2 \mathbf{I}\right]^{-1} \hat{\mathbf{h}}_{C,n,m}, \tag{16}$$

where $\mathbf{R_{hh}} = E(\mathbf{h}_{C,n,m}\mathbf{h}^H_{C,n,m})$.

Let $N = P_t Q_t$. The complexity of the LS method comes from the complex-value division, which is $\mathcal{O}(N)$. The MMSE method adds the matrix inverse and multiplication operations based on the LS method. Therefore, the complexity of the MMSE method is $\mathcal{O}(N^3)$. In contrast, the SAKF method adds scalar KF iterations with only two rounds of circulations and uses the estimated AoAs of JCAS without additional sensing processing. Thus, the complexity of the SAKF method for JCAS system is $\mathcal{O}(N + 2N) = \mathcal{O}(3N)$.

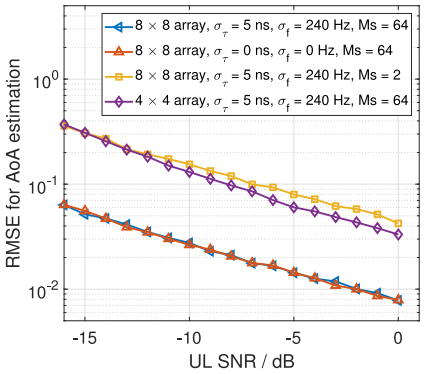

Fig. 3. The AoA estimation RMSE.

IV. Simulation Results

In this section, we present the simulation results of the BERs using the proposed SAKF method, compared with the LS and MMSE methods. The simulation parameters are listed as follows.

The carrier frequency is set to 28 GHz [13], the antenna interval, d_a, is half the wavelength, the array size of the user is $P_r \times Q_r = 1 \times 1$, the number of paths is $L = 2$, $\sigma^2_{\beta_1} = 0.1$, and the reflection factor for the NLoS path follows $\mathcal{CN}(0, 0.1)$. The subcarrier interval is $\Delta f = 480$ kHz, the subcarrier number is $N_c = 256$, and the bandwidth is $B = N_c \Delta f = 122.88$ MHz. The number of packets used for each sensing estimation is $M_s = 64$, and the number of OFDM symbols for each packet is $P_s = 14$. The AoAs for the LoS and NLoS path are $\mathbf{p}^U_{RX,0} = (16^o, 44^o)$ and $\mathbf{p}^U_{RX,1} = (3^o, 32^o)$, respectively. The variance of the Gaussian noise is $\sigma_N^2 = 4.9177 \times 10^{-12}$ W. The transmit power is determined according to the given SNR and σ_N^2. UL SNR is defined as the SNR of each antenna element of BS. According to (3), the UL SNR is expressed as $\gamma_c = P_t^U \sum_{l=0}^{L-1} |b_{C,l} \chi^U_{TX,l}|^2 / \sigma_N^2$.

Fig. 3 presents the AoA estimation RMSE under various array sizes, M_s, CFO and TO. Given the BS array size and M_s, the AoA estimation RMSEs under different TO and CFO are similar. This indicates that the AoA estimation is not prominently impacted by TO and CFO, as discussed in Section III-A. Moreover, when $\sigma_\tau = 5$ ns and $\sigma_f = 240$ Hz, reducing either BS array size or M_s leads to the increase of the AoA estimation RMSE, due to the reduced energy of processing symbols as shown in (5). The AoA estimation RMSE is considerably low even when $M_s = 2$, since the AoA estimation exploits the preamble symbols at all $N_c = 256$ subcarriers.

Fig. 4 presents the normalized MSE (NMSE) for CSI estimation when the BS array size is 8×8, $\sigma_\tau = 5$ ns, and $\sigma_f = 240$ Hz, under 4-QAM modulation. The NMSE is $NMSE = E\{|\hat{h}_i - h_i|^2\}/E\{|h_i|^2\}$, where h_i and $\hat{h}_i$ represent the actual CSI and estimated CSI for each symbol, respectively. As the SNR increases, the NMSE decreases. It is shown that given the SNR, the NMSE of the proposed SAKF-based method is about 17 dB lower than that of the LS method, but 0.8 dB higher than that of the MMSE method.

Fig. 5 demonstrates the BERs using the SAKF, LS, and MMSE methods when the BS array size is 8×8, $\sigma_\tau = 5$ ns,

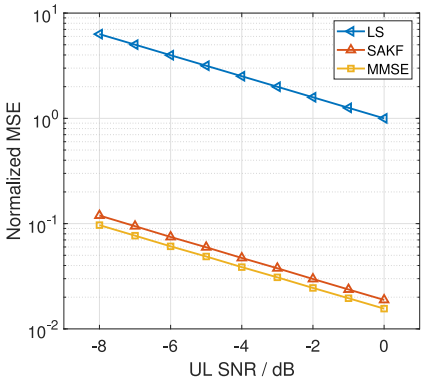

Fig. 4. The Normalized MSE for CSI estimation.

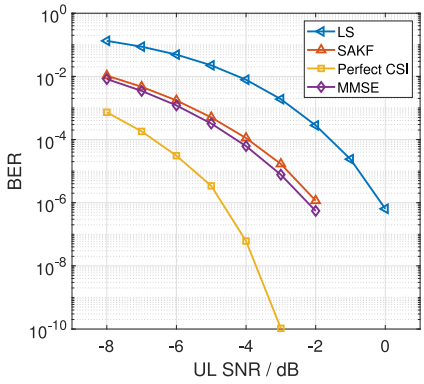

Fig. 5. The BERs using the SAKF, LS, and MMSE methods under 4-QAM modulation.

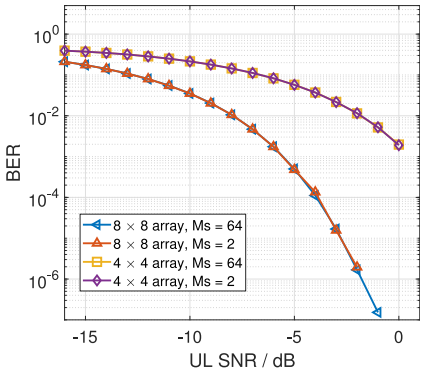

Fig. 6. The BERs of the SAKF method when using 4 QAM under various BS array sizes and M_s.

and $\sigma_f = 240$ Hz, under 4-QAM modulation. The required SNR to achieve the given BER for the SAKF method is about 1.8 dB lower than that for the LS method, but 0.2 dB higher than that for the MMSE method. This is because **Algorithm 1** filters the CSI estimated by the LS method exploiting the estimated AoAs. This indicates that the proposed SAKF method can approach the MMSE method in BER performance with significantly reduced complexity.

Fig. 6 shows the BERs using the SAKF method when $\sigma_\tau = 5$ ns, and $\sigma_f = 240$ Hz, using various BS array sizes and M_s, under 4-QAM modulation. It can be seen that given the BS array size, the BERs under different M_s are similar. This is because M_s only influences the number of symbols for sensing and does not influence the processing SNR of the demodulation over each symbol, while the BS array size directly impacts the total energy of signals for both communication and sensing. Moreover, the AoA estimation RMSEs are considerably small in the studied SNR range, even when the SNR is too low for reliable communication, and the KF-based CSI enhancement can still work normally.

V. Conclusion

In this letter, we propose a SAKF-based UL channel estimation method for JCAS system. The KF exploits the AoAs estimated by MUSIC method as the prior information to refine the LS CSI estimation and improve the reliability of communication. Note that the proposed SAKF-based CSI estimation method can be extended to the cases with other AoA and initial CSI estimation methods. Simulation results show that the SNR required to achieve the given BER for the proposed SAKF-based method is about 1.8 dB lower than the LS method, and about 0.2 dB higher than the MMSE method, while at significantly reduced complexity.

References

[1] F. Liu, C. Masouros, A. Petropulu, H. Griffiths, and L. Hanzo, "Joint radar and communication design: Applications, state-of-the-art, and the road ahead," *IEEE Trans. Commun.*, vol. 68, no. 6, pp. 3834–3862, Jun. 2020.

[2] Z. Feng, Z. Wei, X. Chen, H. Yang, Q. Zhang, and P. Zhang, "Joint communication, sensing, and computation enabled 6G intelligent machine system," *IEEE Netw.*, vol. 35, no. 6, pp. 34–42, Nov./Dec. 2021.

[3] W. Saad, M. Bennis, and M. Chen, "A vision of 6G wireless systems: Applications, trends, technologies, and open research problems," *IEEE Netw.*, vol. 34, no. 3, pp. 134–142, May/Jun. 2020.

[4] J. A. Zhang, K. Wu, X. Huang, Y. J. Guo, D. Zhang, and R. W. Heath, "Integration of radar sensing into communications with asynchronous transceivers," *IEEE Commun. Mag.*, vol. 60, no. 11, pp. 106–112, Nov. 2022.

[5] Y. S. Cho, J. Kim, W. Y. Yang, and C. G. Kang, *MIMO-OFDM Wireless Communications with MATLAB*. Hoboken, NJ, USA: Wiley Publ., 2010.

[6] W. H. T. Rodger E. Ziemer, *Principles of Communications*, 7th ed. New York, NY, USA: Wiley, 2014.

[7] Z. Gong, C. Li, F. Jiang, and M. Z. Win, "Data-aided doppler compensation for high-speed railway communications over mmWave bands," *IEEE Trans. Wireless Commun.*, vol. 20, no. 1, pp. 520–534, Jan. 2021.

[8] G. Liu, A. Liu, R. Zhang, and M. Zhao, "Angular-domain selective channel tracking and doppler compensation for high-mobility mmWave massive MIMO," *IEEE Trans. Wireless Commun.*, vol. 20, no. 5, pp. 2902–2916, May 2021.

[9] R. Zhang, L. Cheng, S. Wang, Y. Lou, W. Wu, and D. W. K. Ng, "Tensor decomposition-based channel estimation for hybrid mmWave massive MIMO in high-mobility scenarios," *IEEE Trans. Commun.*, vol. 70, no. 9, pp. 6325–6340, Sep. 2022.

[10] G. C. Charles K. Chui, *Kalman Filtering: With Real-Time Applications*. Heidelberg, Germany: Springer Int., 2017.

[11] M. Haardt, M. Pesavento, F. Roemer, and M. N. El Korso, "Chapter 15—Subspace methods and exploitation of special array structures," in *Academic Press Library in Signal Processing*, vol. 3, A. M. Zoubir, M. Viberg, R. Chellappa, and S. Theodoridis, Eds. London, U.K.: Elsevier, 2014, pp. 651–717.

[12] Y. Gao, J. Xue, Y. Chang, and Y. Zhang, "An MDL-MUSIC joint time delay estimation method for LTE PRS," in *Proc. Int. Symp. Wireless Commun. Syst. (ISWCS)*, Oct. 2017, pp. 84–89.

[13] "Study on evaluation methodology of new vehicle-to-everything V2X use cases for LTE and NR," 3GPP, Sophia Antipolis, France, Rep. TR 37.885 V15.3.0, 2019.